THE SIZE DEPENDENCE OF CONTRASTS AND NUMBERS OF SMALL MAGNETIC FLUX TUBES IN AN ACTIVE REGION

H. C. SPRUIT
Max-Planck-Institut für Astrophysik, Garching, F.R.G.

and

C. ZWAAN
The Astronomical Institute at Utrecht, The Netherlands

(Received 6 July, 1977; in final form 11 August, 1980)

Abstract. Intensity contrasts and number densities of bright points, knots and pores ranging in size between 0".15 and 4" are studied using high resolution pictures in Mg b_1 of a young active region. On the average, the contrast in the wing of the line increases very strongly with decreasing size, while the continuum contrast increases more slowly. The ratio of contrast in the line to contrast in the continuum increases rapidly with decreasing size. The possibility is explored of using this contrast ratio as an indicator of size. The distribution of the contrast ratio in a part of the active region is used in this way to derive a size distribution of facular points. The resulting distribution has a limited accuracy, but is free from systematic distortion due to selection effects. Validity checks on the method are presented. We measure the size distribution of the pores in the same area, and combine the result with that for the facular points. The combined distribution shows that the surface area covered by magnetic elements with diameter δ has a maximum near $\delta = 0".8$. It increases roughly proportional to δ for $\delta < 0".3$ and falls off as δ^{-1} for $\delta > 1".5$. It is inferred that elements with $0".5 < \delta < 1".6$, which show no conspicuous contrast in the line wing or in the continuum, occupy as much area as the pores, and twice as much as the facular points. We suggest that the changing appearance of a facular area with increasing height of formation reflects at least as much the increasing weight of the small elements in the contrast as a real change in intrinsic properties (such as the diameter) of individual elements. A spatial resolution better than 0".1 may be needed to resolve the individual elements in plages and the chromospheric network.

The observed variation of *continuum* contrast of facular points with size agrees with predictions based on magnetostatic flux tube models if a field strength of about 2000 G is assumed.

1. Introduction

Current observations indicate that the solar magnetic field occurs in concentrations of very different sizes but over a small range of field strength: $2000 \lesssim B \lesssim 3000$ G for sunspots and pores, and $1000 \lesssim B \lesssim 2000$ G for smaller elements (cf. Beckers, 1976; Harvey, 1977). The *brightness* structure depends strongly on size, however. While elements larger than about 1".5 are dark, the smallest elements correspond to the filigree points which appear as bright in the continuum (Dunn and Zirker, 1973) and to the even brighter faculae in the line cores.

There is dispute about the smallest scales at which the brightness structure is cospatial with the magnetic field. According to Simon and Zirker (1974) the magnetic field is not strictly cospatial with the brightness structure and the magnetic elements are rather coarse with typical diameters of 1 to 2". However, Beckers (1975, 1976) found that in the wings of the Mg b_2 line the polarization signal is

Solar Physics **70** (1981) 207–228. 0038–0938/81/0702–0207 $03.30.

cospatial with the brightness signal down to 0".5. Moreover, Ramsey *et al.* (1977) demonstrated that the magnetic structure does consist of small elements with dimensions down to spatial resolution in their magnetograms, viz. $\frac{1}{3}$ arc sec. We adopt the view that down to 0".3 the strong magnetic field ($B \gtrsim 1000$ G) is cospatial with brightness structure in continuum and line wings, viz. either with dark spots or bright filigree.

It has been suggested (Zwaan, 1967; Chapman, 1974; Frazier, 1977) that the solar magnetic elements have the same physical structure: that of magnetic flux tubes in static equilibrium. Indeed models constructed according to this idea (Spruit, 1976, 1977) reproduce some of the main observational features, such as the observed field strengths and the appearance in continuum and line wings, which includes the transition from dark pores to bright faculae near 1", and the center-to-limb behavior of the facular contrast in the continuum. The emission cores in the Ca II and Mg II resonance lines in faculae cannot be explained by the present static models, because the apparent heat dissipation in the chromospheric parts of the flux tubes has not yet been incorporated in the calculations.

Both the observations and the model calculations indicate that the magnetic field strength depends relatively mildly on the diameter of the flux tube. However, the brightness structure in the photosphere and in the chromosphere seems to be very sensitive to the size. The first aim of this paper is to search for the contrast properties of the elements with diameters smaller than about 1" in high resolution filtergrams obtained in Mg I b_1 (5183 Å). We try to establish *mean* properties as a function of the diameter only.

Because of the discrete nature of the magnetic field the average magnetic field strength as measured by a magnetograph is not an adequate measure for the statistical properties of the field. For a sound description are necessary (i) the fractional area covered by the magnetic field, and (ii) *the spectrum of flux tube sizes.* Clearly, the fractional area covered by strong fields varies strongly over the solar surface, and so does the spectrum of element sizes. For instance, in a large young active region there is a broad spectrum of sunspots of different sizes, pores and tiny bright elements. However, in an old remnant of an active region the size spectrum has become limited to small bright elements. One second aim is to estimate the size spectrum for elements from a few arc sec down to the smallest sizes accessible to observations. This first attempt refers to one area in a young active region.

2. Observations and Reduction

The observations consist of 9 high resolution filtergrams taken in the Mg b_1 (5183 Å) line by J. M. Beckers on 8 May 1973 with the universal birefringent filter at the Sacramento Peak Observatory Vacuum Telescope (Beckers *et al.*, 1975). They show a part of the active region McMath 12336, this part was about 3 days old on this date, while its following polarity part was in a phase of rapid dispersal (spots disappearing). The wavelengths were $\Delta\lambda = -1.64, -0.84, -0.44, -0.14, -0.04, 0.07, 0.37, 0.77,$

and 1.57 Å; the band pass was 0.17 Å. The pictures were taken within a few seconds from each other. The $\Delta\lambda = 0.37$ image was reproduced in *Solar Physics* **43**, opposite p. 271. Some results were reported earlier in Beckers (1975, 1976), see also the review by Harvey (1977). An area at $\cos\theta = 0.95$ measuring $29'' \times 38''$ was chosen for further analysis, all results reported below refer to this area. It is located in strong plage of leading polarity, just east of the apparently well developed 'moat' of the leading spot. The maximum facular contrast occurs on the $\Delta\lambda = 0.37$ and -0.44 Å plates. Only the $\Delta\lambda = 1.57$, -0.84, and 0.37 Å plates were analysed, because they show the best resolution, and because for smaller $\Delta\lambda$ the intensities are not easily interpretable due to probable departures from LTE. In Figure 1 three frames used are reproduced. In the following we denote the wavelengths by 1.6, -0.8, and 0.4 for short. The intensity in the photospheric profile, relative to the continuum is at the three wavelengths: 0.88($\Delta\lambda = 1.57$), 0.66 (-0.84), and 0.36 (0.37).

The resolution of the pictures is approximately 0".42 (1.6), 0".32 (-0.8), and 0".38 (0.4) in the area investigated, see Section 3.2.1 for the determination of these values. The measurements were made on intensity maps of the area, produced after microdensitometry with a scanning aperture of 0".09 (the microdensitometry was done on the VAMP machine in Utrecht).

2.1. Selection and measurement of bright points

On the -0.8 plate 59 bright points were *selected* inside the chosen frame of $29'' \times 38''$ on the basis of an *isolated and roundish appearance*. The -0.8 plate was chosen for this selection because it shows the bright points better isolated than the 0.4 plate; on the other hand the definition of the background intensity is easier than on the 1.6 plate, which shows a stronger granulation contrast. Of these 59 points, 57 could be identified also on the 0.4 plate, and 57 on the 1.6 plate. Of each point, at each of the three wavelengths, the diameter d (FWHM) and the *integrated contrast* Q_λ were determined, where

$$Q_\lambda = \int \tilde{q}_\lambda \, \mathrm{d}a \,. \tag{1}$$

Here a is the surface area occupied by the bright point in square arc sec and $\tilde{q}_\lambda$ is the intensity contrast $(I - \langle I \rangle)/\langle I \rangle$ at wavelength λ as a function of position on the plate, relative to the neighbouring background. Note that Q_λ, in contrast to $\tilde{q}_\lambda$, is insensitive to seeing.

3. Diameters

3.1. Wavelength variation

For the selected 59 points we found only a weak variation of diameter with λ. This is illustrated in Figure 2, comparing the diameters of the points at $\Delta\lambda = -0.8$ and 0.4. The ratio of the average diameter at $\Delta\lambda = 0.4$ to that at $\Delta\lambda = -0.8$ is 1.18, which is close to the ratio, 1.16, of the resolution limits on both plates. After correction of the

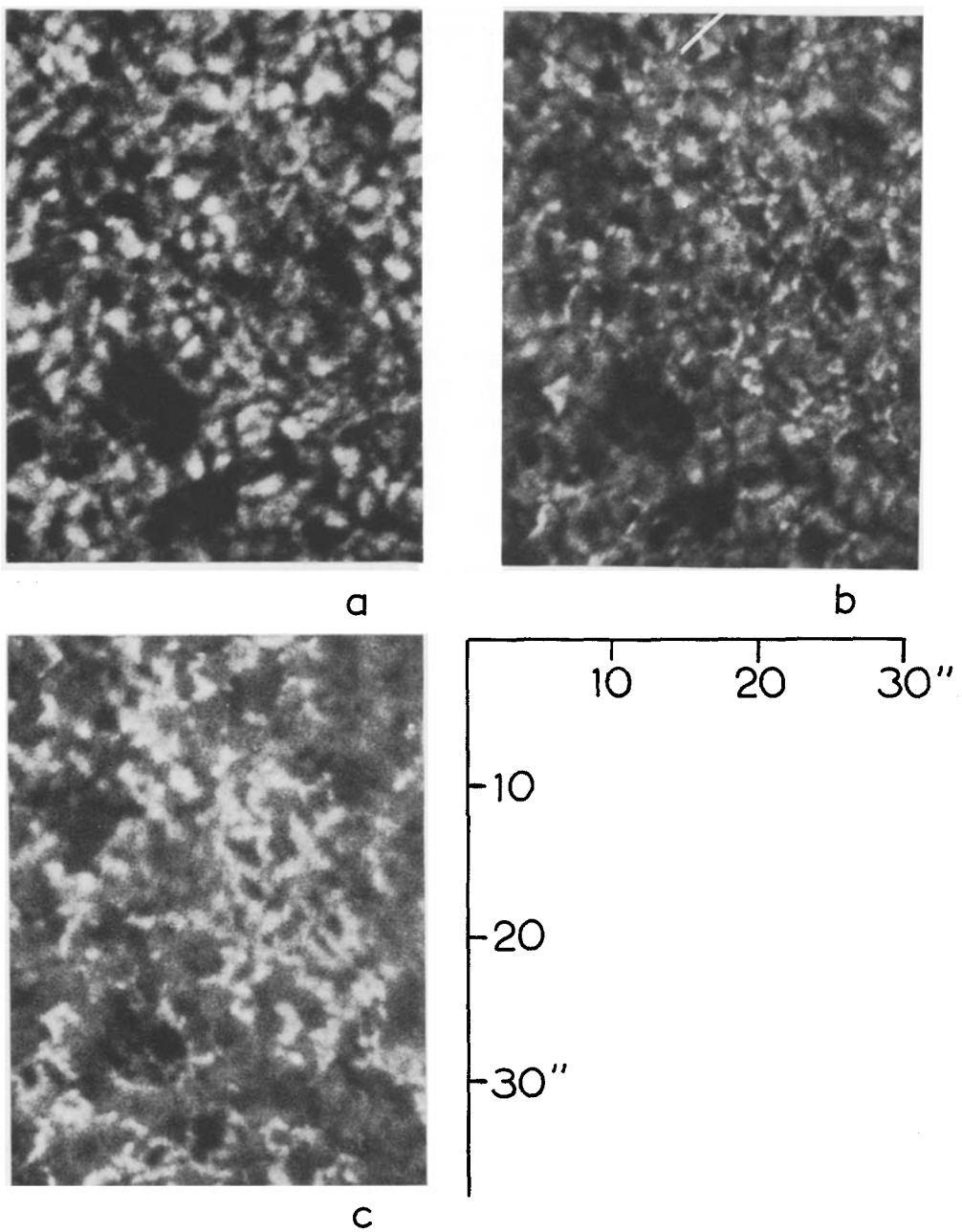

Fig. 1. Part of the filtergrams used for measuring bright points. (a) $\Delta\lambda = 1.57$ Å; (b) -0.84 Å; (c) 0.37 Å.

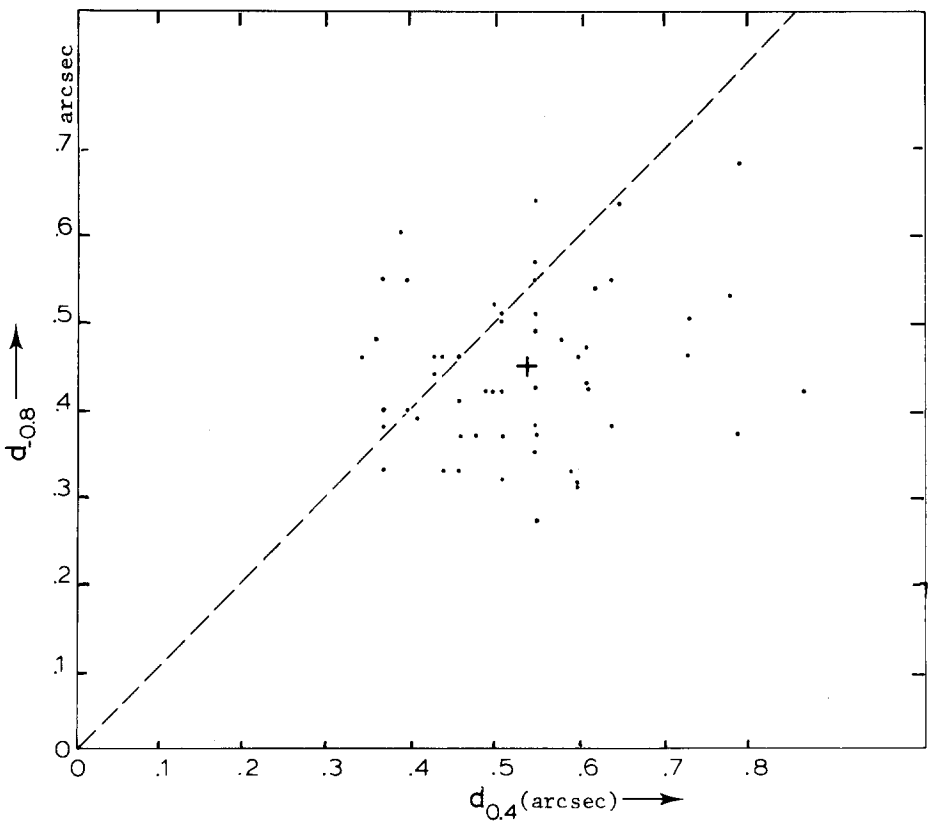

Fig. 2. Diameters of 57 bright points (FWHM) at $\Delta\lambda = 0.4$ and $\Delta\lambda = -0.8$. +: Center of weight of the points.

diameters for finite resolution (see Section 3.2), the average ratio of the intrinsic diameters was found to be 1.20 ± 0.09, where the error represents a formal probable value which does not include the uncertainties in the resolution limits adopted.

This result agrees with the conclusions by Dunn and Zirker (1973) who found that the diameters of filigree elements observed in the wing of Hα increase only weakly towards the line centre. The result agrees also with expectations based on a magnetostatic flux tube picture. In Spruit (1976) we found that flux tubes ranging in diameter between 100 km and 1000 km increase in diameter roughly like $\exp(h/580)$ with height h (km) above the photosphere. If the effective heights of formation of Mg b_1 at $\Delta\lambda = 0.37$ Å and -0.84 Å are 170 and 50 km respectively (computed for the normal photosphere), we expect the diameters on the 0.4 plate to be only 25% larger than on the -0.8 plate (if the structures were fully resolved). At this point a problem arises, since the structure on the 0.4 plate clearly gives a much 'coarser' appearance than on the -0.8 plate. Structures identified *independently* on the 0.4 and -0.8 plate differ in size by a factor of three or more. We must conclude that the structures identified on the 0.4 plate are *not* the same physical objects as

those found independently on the -0.8 plate, though there is a gross spatial coincidence. We return to this point at the end of Section 6.

3.2. Correction of diameters for finite resolution

Most of the points have measured diameters between 0".3 and 0".6. This is fairly close to the resolution limits of the data. It is obvious that the correction for finite resolution has to be done with great care. Even then, corrected diameters of individual points will have large uncertainties. On the other hand we have 59 points available. Thus if there is a sufficiently strong dependence of intrinsic properties (contrasts) on size, we may hope to detect it by statistical means, in spite of the uncertainties.

3.2.1. *Resolution Limits and Measurement Uncertainty*

If the resolution limit were a uniquely determined quantity (uniform across the area studied) and if there were no errors in measuring the diameters, the best estimate of the limit would simply be the smallest diameter measured. This would imply 0".32 at $\Delta\lambda = 0.4$, 0".23 at $\Delta\lambda = -0.8$ and 0".36 at $\Delta\lambda = 1.6$. From our experience while measuring the diameters, we estimate that the uncertainties σ_m in the measurements on the plates are about 0".07 for both $\Delta\lambda = -0.8$ and 1.6, and 0".1 for $\Delta\lambda = 0.4$. These uncertainties are mostly due to the irregularity of shape of the points. We cannot estimate the nonuniformity of seeing quality across the area. We assume here that it is small (the area is 40" wide). Due to this measurement uncertainty, there will be some points with a measured diameter *below* the actual resolution limit of the data.

With the estimated measurement uncertainty we can now make a better estimate of the resolution limit, from the distribution of measured diameters. Denoting the uncertainty by σ, the resolution limit by d_0, and the measured diameter by d, we adjust d_0 such that there are some points with $d_0 - \sigma < d < d_0$, but only few with $d < d_0 - \sigma$. The resulting resolution limits are 0".38 ($\Delta\lambda = 0.4$), 0".32 (-0.8), and 0".42 (1.6). They are determined to within about 0".02 by the present procedure. The numbers of elements in the ranges $d < d_0 - \sigma$ and $d_0 - \sigma < d < d_0$ are, respectively, 1 and 6 (0.4); 2 and 7 (-0.8); 1 and 4 (1.6).

3.2.2. *Correction Procedures*

We could now proceed to correct the diameters for finite resolution assuming, for example, that both the smearing and the intrinsic intensity distribution of the point were gaussian, i.e.

$$d^2 = \delta^2 + d_0^2,$$

where δ would be the FWHM of the intrinsic intensity distribution across the point. This simplistic procedure has two disadvantages:

(a) One has to throw away the information from points with $d < d_0$;

(b) it is difficult to take into account that near $d = d_0$ the values of δ are very uncertain.

Both these problems can be avoided with a slightly more sophisticated correction procedure. With the aid of the known measurement uncertainty, it is possible to estimate the *most probable* value of δ for any value of d even for $d < d_0$ and at the same time estimate the uncertainty in the determination of δ from d. In the Appendix and appropriate procedure is described. It is especially well suited for subsequent statistical analysis (least squares fits) of the contrast data, because it assigns weights to the measurements according to the uncertainty in δ.

4. Contrasts

4.1. Qualitative behavior of size dependence

A number of interesting conclusions can already be drawn from the measurements, without correction for seeing effects. For this purpose, we define the contrast ratios t_1 and t_2 (as a measure of the relative brightness at two wavelengths) by

$$t_1 = Q_{-0.8}/Q_{1.6}\ ; \qquad t_2 = Q_{0.4}/Q_{-0.8}\ . \tag{2}$$

These ratios, as the Q_λ, are largely independent of seeing conditions, since they represent integrated contrasts. If the variation of the diameter of the element with height of formation is small (as we suggested above), the values of t also represent the relative variation of the *intrinsic* contrast of the structure with $\Delta\lambda$. The main source of error in Q_λ is the irregularity of shape of the points, which may account for a scatter of 20%. In addition, on the $\Delta\lambda = 1.6$ plate, the uncertainty in the definition of the background intensity due to granulation yields an error of 20% on this plate, assuming an error of 10% in the background.

In Figures 3 and 4 the measured values of t_1 and t_2 are given in plots of t vs $d_{-0.8}$. There is a large scatter in the values of t for points of a given diameter. For example, t_2 shows a scatter of at least a factor of two. The 20% uncertainty in the values of Q is insufficient to explain this scatter. We can only speculate about the origin of this scatter. It might be because the chromospheric properties of elements of the same diameter differ systematically, or because they are time dependent. There could be a time dependent heating, or a time dependent velocity for example. In the latter case, velocities of the order 20 km s^{-1} would be needed. In any case, we conclude that at a given instant in time there is a real variation in intrinsic (as opposed to seeing induced) contrast among elements of the same diameter. In spite of this spread, t_2 and t_1 show a difference in their dependence on diameter. Whereas t_1 is near unity and varies little with d (perhaps showing a slight increase with d), t_2 decreases from about 7 at $d = 0''.35$ to values of about 2 at $d = 0''.6$. We believe this decrease to be real. It shows that *the increase of brightness with height of formation in faculae is stronger in small elements than in the larger ones.* In addition, this effect becomes pronounced only above a certain height, since t_1 does not show a clear size dependence.

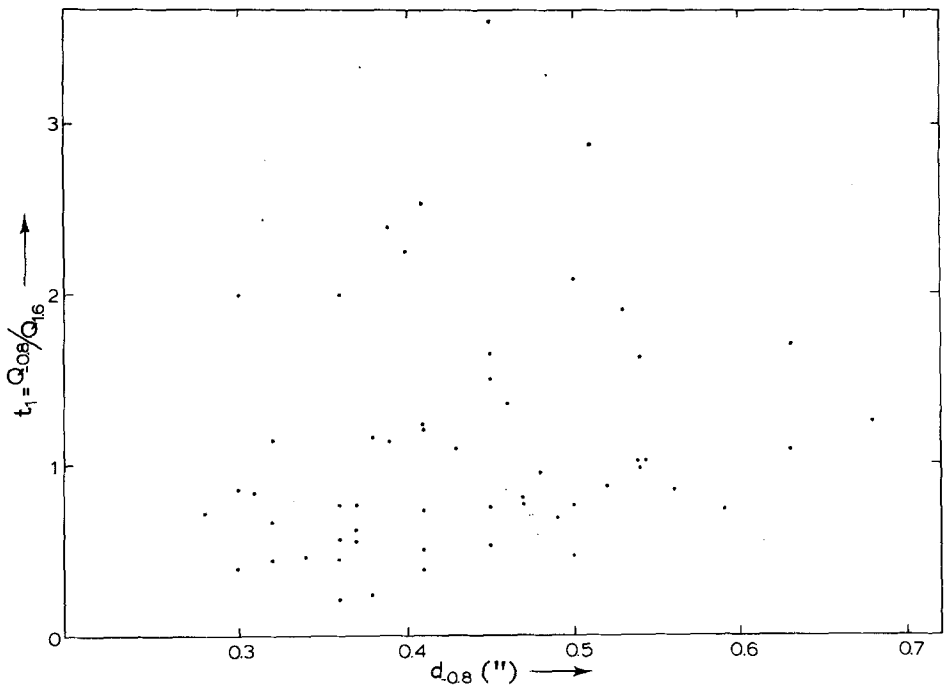

Fig. 3. Contrast ratio $t_1 = Q_{-0.8}/Q_{1.6}$ for 57 bright points, versus the diameter (FWHM) on the $\Delta\lambda = -0.8$ plate.

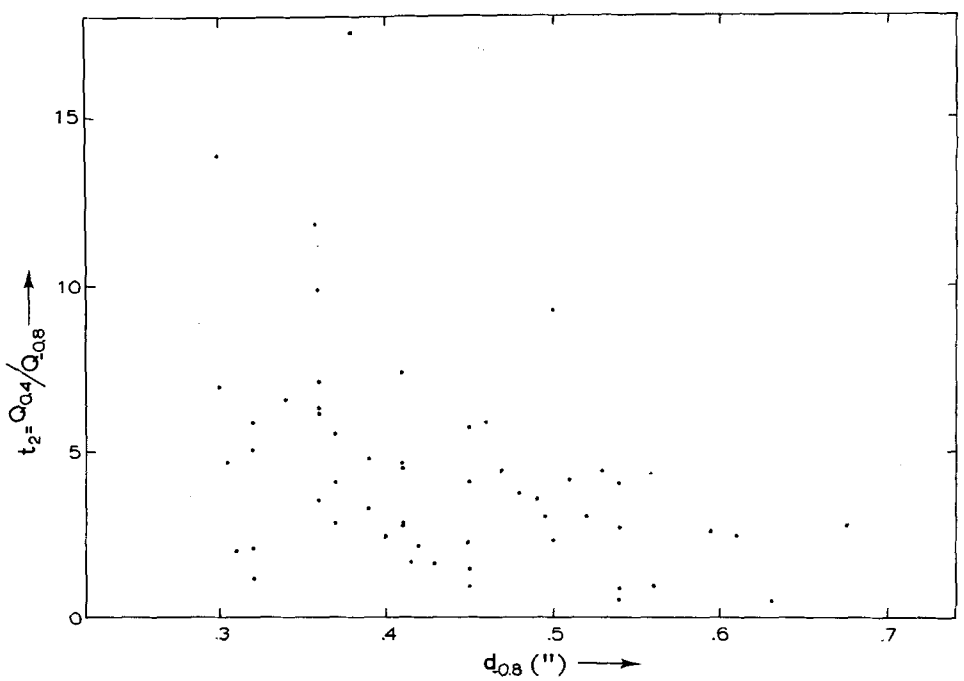

Fig. 4. As Figure 3, but for the ratio $t_2 = Q_{0.4}/Q_{-0.8}$. Note difference in t-scale.

4.2. VARIATION OF CONTRAST BETWEEN 0".1 AND 2"

To make the statements in Section 4.1 more quantitative, we determined estimates of the integrated contrasts $Q_\lambda(\delta)$ by least squares fits. The intrinsic diameters δ were obtained from the measured d's according to the procedure in the Appendix. For δ we take $\delta_{-0.8}$ instead of δ_λ, because the -0.8 plate has by far the best resolution, and has a reliable background intensity. As we found in Section 2 however, the diameters on the three plates are comparable. Assuming a dependence of the form $\log Q_\lambda = a + b \log \delta$, we find (a more elaborate representation is not justified in view of the scatter in the data):

$$\log Q_{1.6} = -0.95 \pm 0.15 + (0.8 \pm 0.3) \log \delta , \tag{3}$$

$$\log Q_{-0.8} = -0.75 \pm 0.10 + (1.1 \pm 0.2) \log \delta , \tag{4}$$

$$\log Q_{0.4} = -0.63 \pm 0.15 + (0.4 \pm 0.3) \log \delta , \tag{5}$$

where the Q_λ are measured in arc sec^2, and δ in arc sec. For the ratio t_2, we find from these relations, $\log t_2 = 0.1 \pm 0.2 - (0.7 \pm 0.3) \log \delta$, which is consistent with a least squares fit using directly the values of t_2 of the points. This direct fit yields:

$$\log t_2 = (0.10 \pm 0.15) - (0.73 \pm 0.25) \log \delta . \tag{6}$$

Similarly, we get for t_1:

$$\log t_1 = (0.20 \pm 0.16) + (0.35 \pm 0.37) \log \delta . \tag{7}$$

From (6) we conclude that the increase of t_2 with decreasing size is indeed significant, while a dependence of t_1 on δ is not significant.

In Figure 5 the intrinsic contrast

$$q_\lambda = Q_\lambda / (\pi \delta^2 / 4) ,$$

determined from (3)–(5) is plotted, assuming again that $\delta_\lambda = \delta_{-0.8}$. It is seen that $q_{1.6}$ and $q_{-0.8}$ do not differ significantly. The apparent difference in contrast between these wavelengths visible in Figure 1 is due to the much stronger granulation contrast at $\Delta\lambda = 1.6$, masking the elements somewhat, and the lower resolution on this plate.

The $\Delta\lambda = 1.6$ plate is close to the continuum; we assume from here on that the contrasts measured on this plate (Equation (3), Figure 5), are representative for the continuum contrast of facular points near 5000 Å.

For $\delta \gtrsim 0".5$ our sample of bright points is rather incomplete because the points, which are identified on the basis of their contrast, are not very conspicuous. To extend the range of sizes, we have also measured the diameter and average contrast of the 12 *pores* in the chosen field, and 6 pores in a nearby field of similar appearance. For this purpose, a pore was defined as a roundish patch that reached a minimum contrast of -20% of the mean intensity, at $\Delta\lambda = 1.6$ Å. The contrast, averaged over the diameter of the pore, is shown in Figure 5. These values are not corrected for stray light. The correction may be considerable since the dark pores are sensitive to

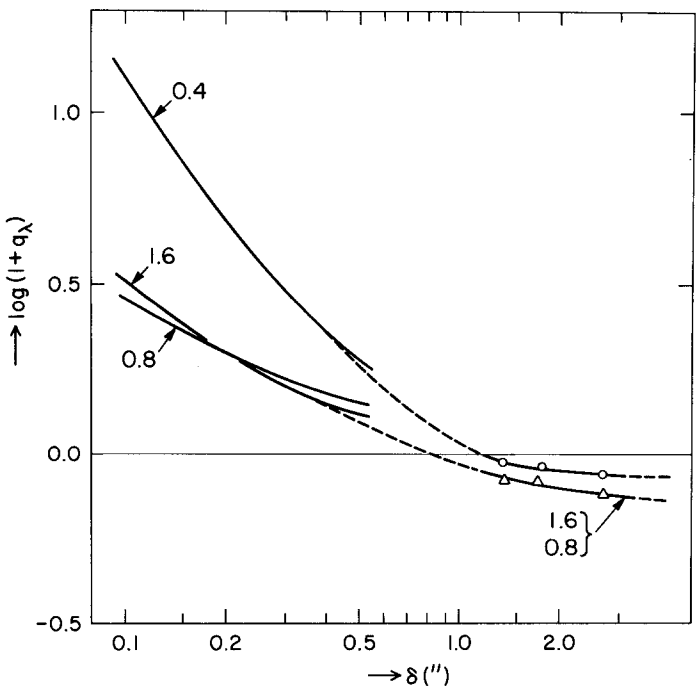

Fig. 5. Intrinsic contrast q_λ as a function of diameter δ derived from measured $Q_\lambda(\delta)$ for facular points (data below 0".5). Also shown are contrasts for pores ($\delta > 1".2$), and the assumed interpolations (broken). The difference between the curves for $\Delta\lambda = 1.6$ and $\Delta\lambda = -0.8$ is not significant.

the extended 'tail' of the smearing function due to light scattered in the instrument.

By interpolation, we infer the probable values of q_λ for elements with $0".5 < \delta < 1".4$. Of course, this procedure makes sense only if we assume that pores and bright points are physically similar things (namely magnetic flux tubes) and that there is a continuous transition in properties.

4.3. Consequences of a size dependent contrast

The high values of $q_{0.4}$ for small elements found here have important consequences for the construction of temperature models of faculae. Models disregarding the strong size dependence will be difficult to interpret since the contrast at different wavelengths is dominated by elements differing considerably in size (see Section 6.3 for quantitative estimates). Average models derived from the contrast in lines of various strengths will be determined by the temperature structure of the larger elements in layers near $h = 0$ ($\tau = 1$). In higher layers however such models would be influenced mainly by smaller elements. Secondly the intensity relative to the continuum becomes very high for small elements. Table I shows the intensity at $\Delta\lambda = 0.4$ and -0.8 relative to the continuum *in the structure*, based on the data of Figure 5. It is seen that emission at $\Delta\lambda = 0.4$ is implied for elements smaller than about 0".4. For comparison, the corresponding values calculated assuming LTE with

TABLE I

Line intensities in Mg b_1 as a function of diameter

δ	0".15	0".2	0".3	0".5	Chapman	Photosphere
$I_{0.4}/I_c$	1.6	1.4	1.2	0.9	0.62	0.36
$I_{-0.8}/I_c$	0.6	0.7	0.7	0.8	0.78	0.66

the recent model 7B13 by Chapman (1977) are shown. This model is based on line profile data at the center of the disk; it properly takes into account the dilution of facular contrast by photospheric light.

5. Facular Points, Knots and Pores

Figure 5 suggests why there is such a clear observational distinction between faculae and pores. Between these classes there seems to be a rather broad range in size, $0".5 < \delta < 1".6$, where the elements are neither conspicuously bright nor dark, neither at the continuum level nor at somewhat greater height. We cannot establish if elements of this size are present in any quantity in the area studied, since we have no magnetic measurements of sufficient resolution. Beckers and Schröter (1968) however found numerous magnetic elements, which they called magnetic knots, in this range of size, with similar properties, in an active region. We define in this paper magnetic knots as elements with sizes between 0".5 and 1".6, and we assume that this definition covers the 'knots' as described by Beckers and Schröter. So on the basis of Figure 5 we divide the presumably continuous range of sizes of magnetic elements into observational categories, by the following definitions:

$\delta < 0".5$ facular points ;

$0".5 < \delta < 1".6$ magnetic knots ;

$1".6 < \delta < 5"$ pores ;

$(\delta > 5"$ spots) .

For a description of pores and the transition to spots we refer to Bray and Loughhead (1964, p. 69).

We will reserve the term 'facula' for the lumps of facular points making up the unresolved 'coarse structure' seen at greater height (Section 6.3).

6. Distribution of Sizes

From the diameters and numbers in the sample of 59 points, the fraction of the surface, $f_a(\delta)$, covered by these points was determined as a function of their diameter. This distribution is shown in Figure 6 (open circles). Since the procedure for selecting the points discriminates against the smallest (unresolved) elements, and

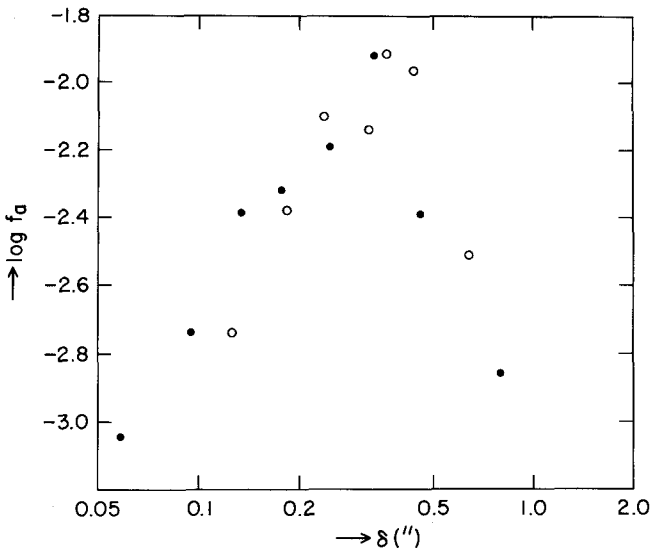

Fig. 6. Fraction of the surface area occupied by sample of 59 facular points, as a function of their diameter (open circles). Solid circles: Same, but derived with indirect method using contrast ratios.

against those with low contrast (the bigger ones), Figure 6 is not representative of the true distribution. An estimate which is not affected by such selection effects, can be made as follows. Contrast values at each position in the entire area studied can easily be measured. The granulation contrast at $\Delta\lambda = -0.4$ is less than at $\Delta\lambda = -0.8$, whereas the opposite is true for bright points. Places where bright points are present are then easily detected by their contrast ratio t_2, which is larger than 1. Since we have established (Equation (6)) an average relation between t_2 and δ, we can estimate from t_2 the *diameter* of the element at the measured position. A measurement at an arbitrary position will in general cover only a fraction of the image of an element. From the amount of contrast at, say, $\Delta\lambda = 1.6$ and the known variation of this contrast with δ (Figure 5) we can calculate how large this fraction is. By adding up the fractions from all locations where the same contrast ratio t_2 is measured, we can construct the total surface area covered, f, as a function of t_2, and by means of the relation $t_2(d)$, as a function of δ. Of course, there is a large scatter in relation (6), so this estimate of f_a is useful only in a statistical sense. We can use the relation to convert a distribution of t_2 values into one of δ values but not for individual estimates of δ. Also, the method assumes that the contrast at any position is due to only one element. Hence we must assume that the individual elements are sufficiently separated so that overlapping of images does not occur. Overlapping is not very likely for the area studied since only about 1% of the surface is covered by bright points.

Due to scatter there is an uncertainty in the mean $t_2(\delta)$ relation which affects the *accuracy* of the results. In addition however, the scatter produces a *systematic*

distortion of the results, because the $t_2(\delta)$ relation is *inverted* to get δ. Therefore, we will first test the validity of the method by applying it to a known situation, for which we take the 59 point sample. We apply the method in exactly the same way as we will apply it to the entire frame (using Equations (8), (11)). The result can be represented in the form of a fractional surface area $f_a(\delta)$ covered by the elements, which can be compared with the one deduced directly from the sample. This is shown in Figure 6. One sees that deviations of the order of 50% in f_a occur, but also that these errors are remarkably small compared to the overall variation of f_a with δ. This shows that the method of using the contrast ratio t_2 to derive the size distribution does not introduce systematic distortions of the results. As an additional test of the method we will check the sensitivity of the results for changes in the assumed $t_2(\delta)$ relation. This is done in Section 6.1.

We now derive the expressions needed to do the actual calculations. We start by measuring how the total contrast in our selected area of $29'' \times 38''$ is distributed over elements with different values of t_2.

For this purpose, define the contrast contribution E at wavelength λ and contrast ratio t by

$$\mathrm{d}E_\lambda(t) = \mathrm{d}t \frac{1}{A} \int_{a_t} \tilde{q}_\lambda \, \mathrm{d}a_t , \tag{8}$$

where t is the ratio of the contrast at two wavelengths (λ_1, λ_2) measured at some point in the active region, $\mathrm{d}t\, a_t$ is the surface area covered by material with a contrast ratio between t and $t + \mathrm{d}t$, and A is the total area of the region measured.

Dividing this contrast contribution by the total contrast per element, i.e. by the average Q_λ for this value of t, we get the number of elements (n) per unit surface area per unit of t:

$$\frac{\mathrm{d}n}{\mathrm{d}t} = \frac{1}{Q_\lambda} \frac{\mathrm{d}E_\lambda}{\mathrm{d}t} . \tag{9}$$

The number density $f_n(\delta)$ per unit diameter δ, and the fraction f_a of the surface covered per unit of δ are then, using the $t_2(\delta)$ relation,

$$f_n(\delta) = \frac{\mathrm{d}n}{\mathrm{d}\delta} = \frac{1}{Q_\lambda} \frac{\mathrm{d}E_\lambda}{\mathrm{d}t} \frac{\mathrm{d}t}{\mathrm{d}\delta} , \tag{10}$$

$$f_a(\delta) = \pi(\delta/2)^2 f_n = \frac{1}{q_\lambda} \frac{\mathrm{d}E_\lambda}{\mathrm{d}\delta} . \tag{11}$$

Lastly, we define the cumulative distribution F_i by

$$F_i = \int_0^\delta f_i \, \mathrm{d}\delta , \tag{12}$$

where i stands for n or a. We use Equation (6) to find the size distribution from the digitised intensity data of the three frames (shown in Figure 1) as follows. First, a precise spatial coincidence of the frames is assured by shifting until optimal correlation of the intensity contrasts is found. Then the mean contrasts $\tilde{q}_{0.4}$, $\tilde{q}_{-0.8}$, and $\tilde{q}_{1.6}$ are calculated in squares of $0''.18^2$, and $t_2 = \tilde{q}_{0.4}/\tilde{q}_{-0.8}$ is calculated if both $\tilde{q}_{0.4}$ and $\tilde{q}_{-0.8}$ are positive. The contribution $\Delta E_{1.6}$ corresponding to an interval Δt_2 (Equation (8)) is formed by adding the values of $\tilde{q}_{1.6}$ of all squares with t_2 in this interval. The results, and the derived size distribution f_a are given in Table II and in Figure 7.

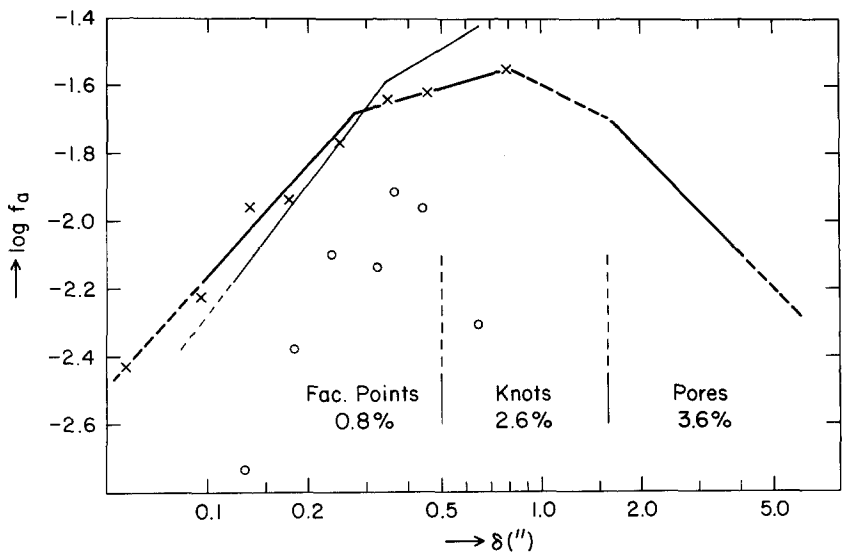

Fig. 7. Distribution of surface area occupied by elements of different sizes. Crosses from measured distribution of the contrast ratio t_2; solid line above $\delta = 1''.6$: From measured areas of pores. Total surface fractions F_f, F_k, F_p for the three categories of elements are indicated. Surface area occupied by elements from 59 point sample (open circles) is shown for comparison. Thin line: Change in f_a resulting from an increase in the slope of the $t_2(\delta)$ relation by one standard deviation.

6.1. Sensitivity to changes in $t_2(\delta)$ relation

Equation (6) shows that the $t_2(\delta)$ relation has an uncertainty of 0.25 in the slope and of 0.15 in the intercept. The intercept uncertainty corresponds to a factor 1.4 in t_2. Since the result is proportional to $\mathrm{d}t/\mathrm{d}\delta$ (Equation (10)), this introduces an uncertainty in $\log f_a$ of 0.15 (independent of δ). One verifies (Figure 7) that this does not influence the basic shape of the distribution. The sensitivity of the results to changes in *slope* of the $t_2(\delta)$ relation is also shown in Figure 7. The thin line shows the results for the relation $\log t_2 = 0.1 - \log \delta$, i.e. for a slope which is one standard deviation higher than relation 6. Again the general shape is affected little.

TABLE II

Measurements for determination of the size distribution

t_2	$\Delta\delta$	$\Delta E_{1.6}$	$Q_{1.6}$	f_a	$\delta('')$
1–2	0".85	4.69×10^{-3}	9.3×10^{-2}	0.028	0.79
2–2.5	0.141	1.29	5.9	0.024	0.45
2.5–3	0.087	1.06	4.8	0.024	0.35
3–4	0.100	1.28	3.6	0.017	0.25
4–5	0.054	7.36×10^{-4}	2.8	0.014	0.18
5–6	0.034	6.15	2.19	0.011	0.13
6–8	0.039	5.69	1.72	0.0059	0.096
8–12	0.034	5.63	1.17	0.0037	0.059

t_2: Contrast ratio $Q_{0.4}/Q_{0.8}$; $\Delta\delta$: Interval in δ corresponding to interval in t_2 according to (8); δ: Diameter corresponding to mean of t_2; $\Delta E_{1.6}$: Measured contrast in interval of t_2; $Q_{1.6}$: Contrast at $\Delta\lambda = 1.6$ according to Equation (3); f_a: Derived size distribution (Equation (11)).

6.2. Discussion of the distribution, extension to pores

Figure 7 gives f_a graphically, compared with the distribution from the 59-point sample of points that were selected and measured individually. It is seen that in the range $0".2 < \delta < 0".5$ the sample contains about half of the elements actually present; outside this range, the selection effects become much stronger. For $\delta \lesssim 0".3$ the slope of the $\log f_a - \log \delta$ relation is approximately 1.2. With the fit given by the straight lines in Figure 7, the total surface fraction occupied by facular points ($\delta < 0".5$) is $F_f \equiv F_a(0".5) = 7.7\times10^{-3}$ of the area measured. To extend the determination of f_a to larger sizes, we measured also the surface occupied by pores. The smallest 'pores' (defined by having a minimum contrast of -20%) have $\delta = 1".2$ (according to the definitions of Section 5 these are actually knots), the largest has $\delta = 4".3$. The surface occupied by pores, f_{ap}, was determined by arranging the pores in order of ascending size, and constructing a plot of the cumulative distribution F_{ap}. A good fit to the data was found to be

$$F_{ap} = 0.032 \ln \delta - 0.015 . \tag{13}$$

With this relation, the area covered by pores is $F_p \equiv F_{ap}(5") - F_{ap}(1".6) = 3.6\times10^{-2}$. By differentiation we find

$$f_{ap} = 0.032\, \delta^{-1} (1".2 < \delta < 4") . \tag{14}$$

This relation is also shown in Figure 7.

If we assume that there is a smooth transition in f_a between facular points and pores, we can estimate the area F_k occupied by the 'knots' ($0".5 < \delta < 1".6$). With the interpolation indicated in Figure 7 (broken line) we infer that $F_k = F_a(1".6) - F_a(0".5) = 0.026$. In other words the knots occupy an area similar to that of pores, and three times that of facular points. Though this conclusion is based on somewhat indirect arguments, it is fully consistent with the results of Beckers and

Schröter (1968). They suggested that most of the magnetic flux of a sunspot returns into the photosphere in the form of magnetic knots, with sizes near 1".3. Observations by Tarbell and Title (1977) also show a high frequency of these knots. The 'dark component' observed by Schoolman and Ramsey (1976) probably refers to what would be large knots and small pores according to our definitions (size measurements were not given by these authors).

The maximum of the distribution in the area investigated seems to occur near the transition between knots and facular points. Since it is observed that pores are not present in the quiet network, it seems likely that the maximum of the distribution shifts to smaller sizes as the active region ages. Consequently, this position of the maximum may also be characteristic only of active regions in a similar stage of evolution.

A magnetogram taken the same day at Kitt Peak National Observatory in Fe I λ 5233, with a resolution of 2".4, shows that the average of the absolute value of the field strength in the area of Figure 1 was 124 G. We can use this value as a check on the distribution in Figure 7. With a total surface area occupied ($f_a(5'')$) of $7 \pm 1\%$, we deduce an average field strength for the elements of 1770 ± 250 G, which though somewhat high, is similar to current determinations of the intrinsic field strength.

6.3. Interpretation of facular structure at different wavelengths

In Section 3.1 we found that bright points identified on the -0.8 plate are found back on the 0.4 plate with nearly the same diameters, yet the overall structure at $\Delta\lambda = 0.4$ gives a much coarser appearance. In this section we try to interpret this behavior, which is found commonly in facular observations (cf., e.g., Dunn and Zirker, 1973), in terms of the results obtained in the previous sections.

From the integrated contrast as a function of diameter given by Equations (3)–(5) the apparent contrast of the images of elements, smeared by finite resolution, can be calculated. This is shown in Figure 8 for $\Delta\lambda = 0.4$ and $\Delta\lambda = 0.8$, assuming resolution limits of 0".37 and 0".32, respectively (as determined in 3.2). At -0.8 the maximum contrast is reached at an intrinsic diameter near the resolution limit; for smaller sizes the contrast drops rapidly, and for $\delta \approx 0''.1$ it becomes comparable to the background noise (granulation) of the plate. At $\Delta\lambda = 0.4$ however, the apparent contrasts are much higher, and their decrease with decreasing size is slower, so that even elements smaller than 0".1 are expected to produce a clearly detectable intensity enhancement. If there is a sufficient number of elements with $\delta < 0''.1$, and especially if the elements have a tendency of clumping, overlapping of unresolved images is much more likely to occur on the 0.4 plate than on the -0.8 plate. Thus while at -0.8 we see *individual* (nearly) resolved elements, at 0.4 we may see in addition to the bigger elements that show up on both plates, clumps of unresolved elements containing several small elements.

As an example we consider the following model for such a clump. The clump is an area of $(2'')^2$ in which the distribution of Figure 7 is locally enhanced by a factor of 7. The average field strength of this 'clump' would then be 390 G (assuming that the

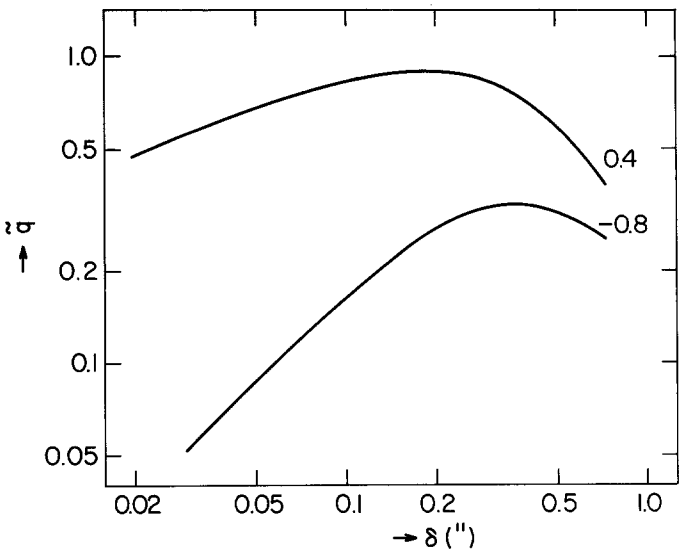

Fig. 8. Apparent contrast of facular points as a function of true diameter, obtained from intrinsic contrast (Figure 5) by smearing with 0".32 ($\Delta\lambda = 0.8$) and 0".37 ($\Delta\lambda = 0.4$).

clump does not contain pores). From the size distribution we find that there would typically be 4 elements detectable on the -0.8 plate ($0''.1 < \delta < 0''.6$) in the clump; their (smeared) images would occupy 14% of its surface. Extrapolation of f_a suggests that there may be as many as 10 elements below 0".1 with sufficient contrast at $\Delta\lambda = 0.4$; their images occupy an additional 27% on this plate, while they are invisible at $\Delta\lambda = 0.8$. The images would occupy 41% of the area at $\Delta\lambda = 0.4$, vs 14% at $\Delta\lambda = -0.8$. Thus overlapping of images is not strong at $\Delta\lambda = -0.8$ but it is almost certain to occur at $\Delta\lambda = 0.4$.

This explanation of the 'coarse structure' at $\Delta\lambda = 0.4$ depends strongly on the contrast and number of elements below 0".1, which admittedly is not determined very well by our data. If it is correct, however, it also suggests a natural explanation of the finding by Simon and Zirker (1974), that magnetic structures observed in the core of Ca I 6103 have characteristic sizes of 1".5 or bigger, as opposed to filigree sizes of 0".2–0".5. They point out that this apparent difference is too large to be explained by the increase with height of the diameter of a magnetic flux tube. It could, however, be due to a coarse structure in 6103 similar to that in Mg b_1 at 0.4 Å, showing structures (clumps) that are physically different from the filigree.

7. Comparison with Flux Tube Models

As we discussed in Section 4.1 (see also Table I) the strong size dependence of the intensity contrast starts at some height ($h \gtrsim 100$ km probably) above the local $\tau = 1$ level. This indicates that the additional sources of heat needed to explain the facular contrasts, become effective only above that height. Near the continuum level this

heating may not be important, the contrast at this level is then due only to effects of radiative transfer in the peculiar geometry of the magnetic flux tube. In Spruit (1976, 1977, Papers I and II hereafter) we showed that a net positive *continuum* contrast in small tubes naturally follows from the condition of lateral energy balance with the normal convection zone surrounding the tube. Models show a transition between dark and bright structures in the continuum near diameters of 1″ (if the Wilson depression is 200 km), which corresponds to the observations (Paper II). The peculiar center to limb variation of the continuum contrast of faculae can be explained as due to geometrical effects of radiative transfer in the tube (Paper I).

The variation of continuum contrast with diameter found in Section 4 can be used as a further test of these tube models. We compare in the following the $\Delta\lambda = 1.6$ data of Figure 5 with models as discussed in Paper II (Section 7). These models form a family with two parameters; the Wilson depression (z_w), which is connected with the field strength of the tube, and the radius (r_0). The family is further characterized by a horizontal mixing length outside the tube according to Paper II, Equation (45a) and a reduction of the vertical convective efficiency to 0.106 (Paper II, Section 7.1). To fix the Wilson depressions of the tubes, we assume here a constant value of the magnetic field strength B_0 (measured at $\tau = 1$), independent of the radius of the tube. This results in a dependence of z_w on r_0, which is shown in Figure 9 for three values of B_0: 1600, 2000, and 2400 G. We note that a given B_0 does not imply a fixed z_w, since the internal gas pressure of the tube varies with r_0 due to differences in thermal structure

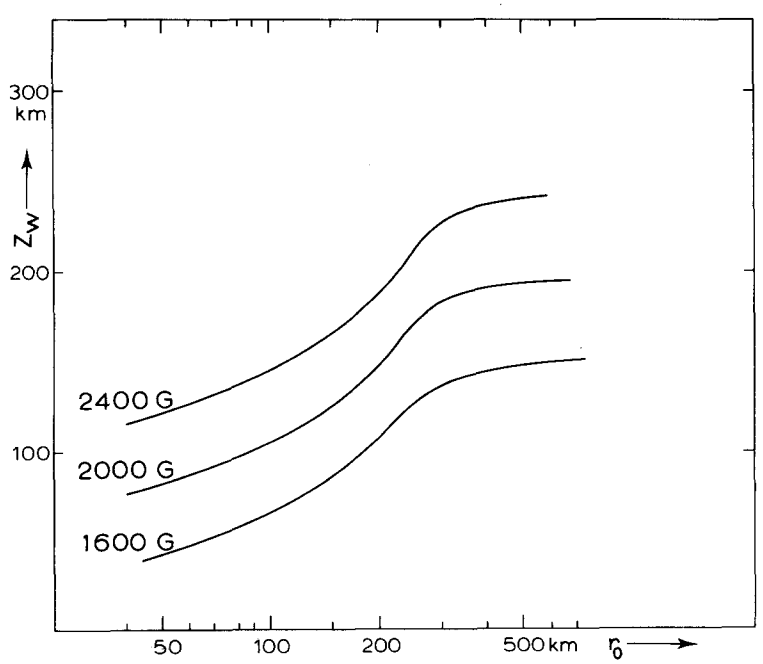

Fig. 9. Dependence of Wilson depression on tube radius for fixed values of the field strength at $\tau = 1$, for magnetostatic tube models discussed in text.

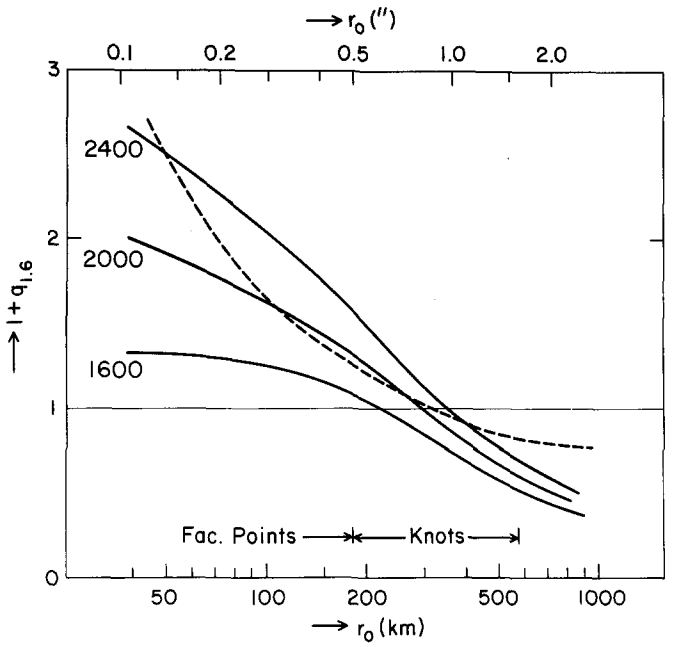

Fig. 10. Continuum intensity averaged over cross section of tube as a function of the radius, for fixed values of the field strength (solid lines). Broken: Continuum intensity derived from present measurements (see Figure 5).

(Paper I). In Figure 10, the model contrast q_λ of the tube at 5183 Å, averaged over the cross section of the tube is shown, as it would be seen at the center of the solar disk. It was calculated from the temperatures of the model with the approximation

$$1+q_\lambda = \frac{2}{r_0^2 I_\lambda^p} \int_0^{r_0} B_\lambda[T(r, z_w)]\, r\, \mathrm{d}r, \tag{15}$$

where B_λ is the Planck function and I_λ^p the normal photospheric intensity. Thus we assume that at the disk center the walls of the tube do not contribute (for justification see Paper I), and we use the Eddington Barbier approximation. The $q_{1.6}$ curve from Figure 5 is also shown in Figure 10 for comparison. It is seen that for facular points the models agree reasonably well with the observational results if we assume a field of about 2000 G. Such a field strength is indicated by observations (Stenflo, 1973; Chapman, 1977) though measurements by Harvey and Hall (see Harvey, 1977) indicate somewhat smaller values. A discrepancy occurs for pores: since the field of pores is probably not higher than 2000 G, the models are clearly too dark in this range of size. This may indicate that the measurements of the pores contain much stray light. On the other hand, the error may well be due to the diffusion approximation used for calculating the energy transfer in the models. In a large tube ($r_0 \gtrsim$ 500 km) the radiation from the walls which heats the central parts of the tube travels

a large distance compared to the scale height of the atmosphere. A diffusion approximation underestimates the heating effect under such circumstances.

8. Discussion and Conclusions

We find a strong dependence of facular contrast both on size and on λ in Mg b_1. The dependence of contrast on size has important consequences for the interpretation of facular observations. Since in the continuum the size dependence is only weak, observations at different wavelengths *do not show the same physical objects.* At wavelengths where the facular contrast is strong one sees much smaller elements than near the continuum. This makes it necessary to distinguish between facular models for different sizes. Near the continuum most of the contrast seems to be due to elements that are just resolvable ($\delta \approx 0''.2$, Dunn and Zirker, 1973). Our results indicate however that an important part of the typical chromospheric facular contrast in Mg b_1 could be due to elements with $\delta \lesssim 0''.1$. This implies that it would be impossible to resolve the facular structure with present observational means.

We find that the contrasts and numbers of facular points as functions of size can be joined smoothly to those of pores. This lends support to the idea that these phenomena have a common physical basis, and that there is a gradual transition in properties from small bright elements to the larger dark ones. In line with current magnetic observations of the same phenomena we assume that these structures correspond to magnetic flux tubes. This has been suggested previously by Zwaan (1967). With this assumption our results indicate that flux tubes with sizes between $0''.5$ and $1''.6$ carry a large fraction of the total magnetic flux in an active region. They are hard to observe however because they have small contrasts in the line and the continuum. We call them magnetic knots, following Beckers and Schröter (1968).

Construction of facular models from observations of average contrasts must rely on more indirect methods, in which knowledge of the *size distribution* of elements is essential.

As to the origin of the contrast, we have shown that *near the continuum level* the contrast at the disk center can be explained satisfactorily with magnetostatic flux tube models in energy balance with the convection zone, without invoking additional sources of heat. Thus only the explanation of the contrast seen in the spectral lines may need an additional heating process, which reduces the energy requirements considerably.

The maximum of the distribution of sizes (as expressed in the surface area occupied) near $0''.8$, is probably typical only of young active regions, since the larger elements like pores do not occur in the network. The maximum in the network may be located at smaller sizes.

We have used only the average properties of the tubes of a given size; there is however an important intrinsic scatter. This scatter may be related to the time dependence of contrast in the facular structure, observed by Dunn and Zirker (1973), Mehltretter (1974) and Muller (1977).

Acknowledgements

We thank Mr. E. J. B. van der Zalm who developed and applied the programs for all data handling needed in this work. We are indebted to Dr J. W. Harvey for putting at our disposal the KPNO magnetogram used in Section 6. We thank the referee for his valuable criticism, which led to substantial improvements. This work was started while one of the authors (H.C.S.) was employed by the Netherlands Organisation for the Advancement of Pure Research (ZWO).

Appendix: Correction of Diameters for Finite Resolution

Let D be the diameter of an image on the plate, d its measured value, and σ the measurement uncertainty. Since the resolution limit is not relevant to the process of physically measuring diameters, D can at this stage have any value >0. Let the measurement process be such that the chance of measuring a value d for a given D is $P_\sigma(d, D)$. P will in general be finite for all $d, D>0$. If nothing else were known about the images studied, the best estimate D_e of the image diameter would be

$$D_e = \int_0^\infty DP_\sigma(d-D)\,\mathrm{d}D\,. \tag{16}$$

It makes sense, however, to include our knowledge that the plate has a resolution limit d_0, such that no images with $D<d_0$ exist. Let $Q(D)$ be the chance that an image on the plate has a diameter D. Then the chance of measuring a value d, *including this knowledge*, is

$$P'_\sigma(d, D) = \frac{1}{W} P_\sigma Q\,, \tag{17}$$

where

$$W(d) = \int_0^\infty P_\sigma Q\,\mathrm{d}D\,, \tag{18}$$

and the best estimate of D would be

$$D_e(d) = \int_0^\infty DP'_\sigma\,\mathrm{d}D\,. \tag{19}$$

Of course, $Q(D)$ is not known, since it depends on the intrinsic size distribution. For the present purpose, however, it is sufficient to take into account just the important fact that Q is zero below the resolution limit. So we take $Q(D)=0$ $(D<d_0)$, and

$Q(D) = 1(D > d_0)$. Then

$$D_e(d) = \frac{1}{W} \int_{d_0}^{\infty} DP_\sigma \, \mathrm{d}D \,. \tag{20}$$

If we assume $D^2 = \delta^2 + d_0^2$ (gaussian profiles), this implies

$$\delta_e(d) = \frac{1}{W} \int_{0}^{\infty} \delta P_\sigma \frac{\partial D}{\partial \delta} \mathrm{d}\delta \,. \tag{21}$$

This is the corrected diameter we use in this study. For P_σ we have used a simple square distribution depending on $D - d$ only:

$$\begin{aligned} P_\sigma &= 1/(2\sigma) \qquad -\sigma < d - D < \sigma \\ &= 0 \qquad\qquad \text{else} \,. \end{aligned} \tag{22}$$

The quantity $W(d)$ is interpreted as the *weight* of the measurement. It is near unity for $d \gg d_0$ and near zero for $d \ll d_0$. This interpretation follows from (18), which shows that $W(d)$ is proportional to the (unconditional) likelihood of measuring a value d.

References

Beckers, J. M.: 1975, *Bull. Am. Astron. Soc.* **7**, 346.

Beckers, J. M.: 1976, in D. J. Williams (ed.), *Physics of Solar-Interplanetary Environments*, Vol. 1, American Geophysical Union.

Beckers, J. M. and Schröter, E. H.: 1968, *Solar Phys.* **4**, 142.

Beckers, J. M., Dickson, L., and Joyce, R.: 1975, *Appl. Opt.* **14**, 2061.

Bray, R. J. and Loughhead, R. E.: *Sunspots*, Chapman and Hall, London.

Chapman, G. A.: 1974, *Astrophys. J.* **191**, 255.

Chapman, G. A.: 1977, *Astrophys. J. Suppl.* **33**, 35.

Dunn, R. B. and Zirker, J. B.: 1973, *Solar Phys.* **33**, 281.

Frazier, E. N.: 1977, in R. Contopoulos (ed.), *Highlights of Astronomy* **4**, Part II, 255.

Harvey, J. W.: 1977, in R. Contopoulos (ed.), *Highlights of Astronomy* **4**, Part II, 223.

Mehltretter, J. P.: 1974, *Solar Phys.* **38**, 43.

Muller, R.: 1977, *Solar Phys.* **52**, 249.

Ramsey, H. E., Schoolman, S. A., and Title, A. M.: 1977, *Astrophys. J.* **215**, L41.

Schoolman, S. A. and Ramsey, H. E.: 1976, *Solar Phys.* **50**, 25.

Simon, G. W. and Zirker, J. B.: 1974, *Solar Phys.* **35**, 331.

Spruit, H. C.: 1976, *Solar Phys.* **50**, 269 (Paper I).

Spruit, H. C.: 1977, *Solar Phys.* **55**, 3 (Paper II).

Stenflo, J. O.: 1973, *Solar Phys.* **32**, 41.

Tarbell, T. D. and Title, A. M.: 1977, *Solar Phys.* **52**, 12.

Zwaan, C., 1967, *Solar Phys.* **1**, 478.